02

# Single-Gap Superconductivity of $(K_{0.8}Na_{0.2})_{0.9}Fe_{1.7}Se_2$ and $K_{0.8}Fe_{1.7}(Se_{0.73}S_{0.27})_2$ Selenides Determined using Multiple Andreev Reflection Effect Spectroscopy

© T.E. Kuzmicheva<sup>1</sup>, S.A. Kuzmichev<sup>2,1</sup>, A.D. Ilina<sup>1</sup>, I.A. Nikitchenkov<sup>2,1</sup>, A.I. Shilov<sup>1</sup>, E.O. Rakhmanov<sup>3,1</sup>, I.V. Morozov<sup>3</sup>

Moscow, Russia

<sup>2</sup> Faculty of Physics, Moscow State University,

Moscow, Russia

<sup>3</sup> Department of Chemistry, Moscow State University,

Moscow, Russia

E-mail: kuzmichevate@lebedev.ru

Received March 6, 2025 Revised March 6, 2025 Accepted May 5, 2025

We have comprehensively studied the structure of the superconducting order parameter of  $(K_{0.8}Na_{0.2})_{0.9}Fe_{1.7}Se_2$  and  $K_{0.8}Fe_{1.7}(S_{0.73}Se_{0.27})_2$  iron selenides with critical temperatures  $T_c \approx 27-31\,\mathrm{K}$ . Using incoherent multiple Andreev reflection effect spectroscopy of planar "break-junctions", in both compounds a development of a single-gap superconductivity and a bulk nature of the observed superconducting gap were shown, its magnitude and temperature dependence have been determined. The characteristic ratio  $2\Delta(0)/k_BT_c \approx 4.1-4.6$  obtained is almost similar for both compounds and points to a strong coupling in the electron bands.

**Keywords:** high-temperature superconductivity, iron-based superconductors, tunneling spectroscopy, multiple Andreev reflections, superconducting order parameter.

DOI: 10.61011/PSS.2025.06.61704.8HH-25

# 1. Introduction

Iron-containing superconductors based on alkali metal selenides of the  $A_x$ Fe<sub>2</sub>Se<sub>2</sub> (A — Na, K, Rb, Cs, Tl) family discovered in 2010 [1] are still extremely understudied due to a number of features that hinder experiments very Properties of materials belonging to this family degrade very fast in the presence of even trace amounts of water and oxygen vapor due to the presence of alkali metal atoms that intercalate superconducting (SC) FeSe blocks. Therefore, preparation and mounting of the sample, and all experimental process stages shall be carried out in a protective gas atmosphere. Natural phase separation is another unique feature of selenides of the  $A_x$ Fe<sub>2</sub>Se<sub>2</sub> family. Possible number of co-existing phases and their structure in selenides with various compositions are still the subject of discussion; however, the main volume of a crystal has been found to be occupied by an insulating antiferromagnetic (AFM) phase with a A<sub>0.8</sub>Fe<sub>1.6</sub>Se<sub>2</sub> crystal structure (so-called 245-phase), where the iron vacancies form a superlattice with  $a^* \approx \sqrt{5}a$  (a — the lattice constant of phase 122). AFM crystallites of the 122-phase of  $A_x$ Fe<sub>2</sub>Se<sub>2</sub> about 1-5  $\mu$ m in thickness are formed at the AFM-phase boundaries ([2–5] as overview). Both phases have a multilayer crystal structure consisting of antifluoritelike FeSe blocks intercalated by alkali metal atoms.

Superconductivity occurs in a narrow valence range of Fe 1.93–2.01 [6], while the critical SC-transition temperature varies stepwise from  $T_c^{\text{max}} \approx 33 \,\text{K}$  to zero even when the amount of A or Fe varies a little [3]. On the other hand, with isovalent substitution (Se, S), the superconductivity is suppressed constantly, and  $T_c$  forms a doping "semidome" [7,8].

The presence of the only one band crossing the Fermi level and, consequently, a development of single-gap superconductivity below  $T_c$  may be noted as another feature of some  $A_x \text{Fe}_2 \text{Se}_2$  compounds that distinguishes them from most iron-containing superconductors. Angle-resolved photoemission spectroscopy (ARPES) investigations have shown that an excessive amount of electrons per Fe atom [9] on the Fermi surface of some  $A_x \text{Fe}_2 \text{Se}_2$  compositions leads to the absence of hole pockets around  $\Gamma$ -point, whereas only electron pockets slightly corrugated along the  $k_z$ -direction are observed around M-point of the Brillouin zone [10–14]. Below  $T_c$ , the only one isotropic SC gap with a high characteristic ratio  $2\Delta(0)/k_BT_c=7-9$  opens in these sheets of Fermi surface [14].

In [10,11,13], for some  $A_x$ Fe<sub>2</sub>Se<sub>2</sub> compositions, an electron pocket with a small phase volume was also allowed around  $\Gamma$ -point [10–12], where the second gap opens in the SC state.

It is also interesting that in a crystal with a similar composition,  $(K_{0.8}Na_{0.2})_{0.8}Fe_{1.7}Se_2$ , grown by the same method, ARPES was used to observe significant variation of

<sup>&</sup>lt;sup>1</sup> Lebedev Physical Institute, Russian Academy of Sciences,

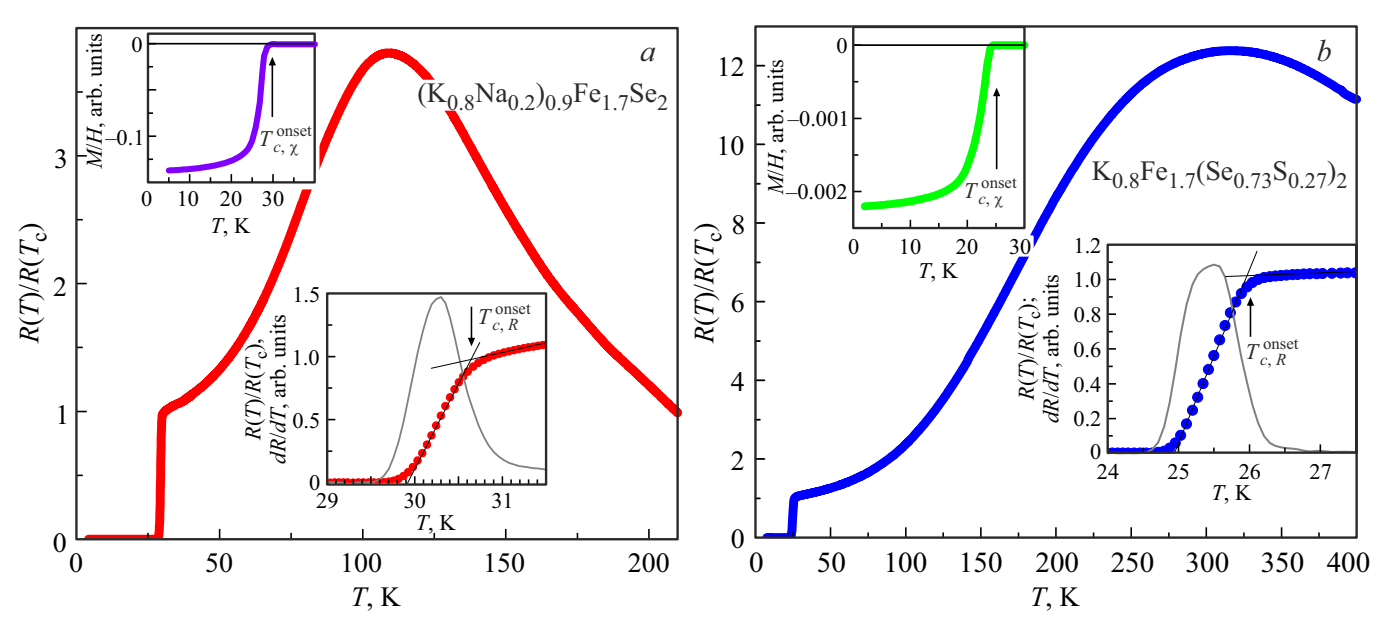


**Figure 1.** Temperature dependence of the resistance of samples a)  $(K_{0.8}Na_{0.2})_{0.9}Fe_{1.7}Se_2$  and b)  $K_{0.8}Fe_{1.7}(Se_{0.73}S_{0.27})_2$ . The lower insets show the details of SC transitions (circles) and the corresponding derivatives dR/dT (lines). Critical temperatures for  $(K_{0.8}Na_{0.2})_{0.9}Fe_{1.7}Se_2$  are  $T_{c,R}^{onset} \approx 31.7 \, \text{K}$ ,  $T_c^{dR/dT} \approx 31.2 \, \text{K}$ ; for  $K_{0.8}Fe_{1.7}(Se_{0.73}S_{0.27})_2$  are  $T_{c,R}^{onset} \approx 27.4 \, \text{K}$ ,  $T_c^{dR/dT} \approx 26.9 \, \text{K}$ . Dependences of magnetic susceptibility on temperature are shown in the upper insets. Corresponding critical temperatures are  $T_{c,\chi}^{onset} \approx 29.3 \, \text{K}$  for  $(K_{0.8}Na_{0.2})_{0.9}Fe_{1.7}Se_2$ ,  $T_{c,\chi}^{onset} \approx 24.5 \, \text{K}$  for  $K_{0.8}Fe_{1.7}(Se_{0.73}S_{0.27})_2$ .

the core levels and valence band with temperature [15] that was uncharacteristic of the conventional superconductor.

For theoretical explanation of the aspects of Cooper pairing in iron-containing superconductors, models on the basis of interaction through spin  $(s^{+-})$  [16] and orbital  $(s^{++})$  fluctuations [17] were proposed. Gap structure of iron selenides without a hole pocket in the  $\Gamma$ -point is addressed in detail in [18–20] within the  $s^{++}$ - and  $s^{+-}$ -models, as well, within the  $s^{\pm}$  approach [21,22] with orbital selectivity taken into account.

For potassium selenides with isovalent substitution,  $(K_{0.8}Na_{0.2})_{0.9}Fe_{1.7}Se_2$  and  $K_{0.8}Fe_{1.7}(S_{0.27}Se_{0.73})_2$ , studied in our work, the Fermi surface topology and data about the presence/absence of an electron pocket in  $\Gamma$ -point are not available in the literature, therefore the question concerning the number of bands on the Fermi surface is still open. In general, for selenides of the  $A_xFe_2Se_2$  family, there are virtually no full-scale systematic investigations of the SC-gap structure and its evolution when the composition and degree of substitution are varied.

This study used the incoherent multiple Andreev reflection effect (IMARE) spectroscopy to study the I(V)- and dI(V)/dV-characteristics of tunneling contacts formed in the  $(K_{0.8}Na_{0.2})_{0.9}Fe_{1.7}Se_2$  and  $K_{0.8}Fe_{1.7}(S_{0.27}Se_{0.73})_2$  samples. On the basis of significant data statistics, it was shown that single-gap superconductivity is established below  $T_c$ , the magnitude  $\Delta(0)$ , characteristic ratio  $2\Delta(0)/k_BT_c$  and temperature dependence of the SC-gap were determined. Similarity of the SC-gap structure and realization of strong coupling in electron bands are shown.

## 2. Experiment details

Single crystals with nominal composition,  $(K_{0.8}Na_{0.2})_{0.8}Fe_2Se_2$ and  $K_{0.8}Fe_2(S_{0.25}Se_{0.75})_2$ , formed by means of three-stage synthesis. Preparation of reaction mixture for all stages, selection and preparation of crystals for the experiments were carried out in an argon glove box with oxygen and water vapor concentration below 0.1 ppm. At the first stage for FeSe and FeS<sub>0.25</sub>Se<sub>0.75</sub> synthesis, reagents in the stoichiometric ratio were triturated in a mortar and placed in evacuated quartz tubes. For FeSe synthesis, a tube was heated in a muffle furnace to 750 °C and held for 48 h. To prepare FeS<sub>0.25</sub>Se<sub>0.75</sub>, a tube was heated in a muffle furnace to 700 °C and held for 24 h. At the second step, Na<sub>0.8</sub>Fe<sub>2</sub>Se<sub>2</sub>, K<sub>0.8</sub>Fe<sub>2</sub>Se<sub>2</sub> and  $K_{0.8}Fe_2(S_{0.25}Se_{0.75})_2$  precursors were prepared by heating the alkali metal and powders synthesized at the first step with the mole ratio 0.8:2. Heating was performed in evacuated quartz tubes during 6h at 340, 380 and 400°C for precursors with three above-mentioned compositions, At the final stage, the prepared product respectively. was thoroughly triturated in an agate mortar and mixed in the required ratio to prepare  $(K_{0.8}Na_{0.2})_{0.8}Fe_2Se_2$  and  $K_{0.8}Fe_2(S_{0.25}Se_{0.75})_2$ . Crystals were synthesized from the melt of their own components. For this, accurately weighed quantities were placed in alundum crucibles that were then sealed in evacuated double quartz tubes. The tubes were heated in a furnace up to 1050 °C, held for 10 h, then cooled to  $750 \,^{\circ}\text{C} \, [(K_{0.8}\text{Na}_{0.2})_{0.8}\text{Fe}_2\text{Se}_2]$  or

 $730\,^{\circ}\text{C}~[K_{0.8}\text{Fe}_2(S_{0.25}\text{Se}_{0.75})_2]$  at a rate of  $6\,^{\circ}\text{C/h}$  and water quenched.

In all cases, large rectangular platelet single crystals with the length of the side up to 8 mm were formed. Microstructure analysis of the prepared crystals was carried out using the electron microprobe analysis with an energy-dispersive detector (INCA X-sight, Oxford Instruments) mounted on the JEOL JSM 6490 LV electron microscope. Quantitative spectral analysis was carried out using INCA (Oxford Instruments) software. Crystal composition was calculated by averaging over  $8\!-\!10$  points for 5 crystals based on overlapping 95% of confidence intervals for all elements and was equal to  $(K_{0.82(2)}Na_{0.17(2)})_{0.89(3)}Fe_{1.69(2)}Se_{2.00(2)}$  (hereinafter referred to as KNFS) and  $K_{0.78(7)}Fe_{1.70(4)}(Se_{0.73(3)}S_{0.27(2)})_2$  (KFSS).

Figure 1 shows the temperature dependences of resistances of the KNFS and KFSS samples measured by the four-point method. At low temperatures, the SC-phase shunts the sample (R=0). Critical temperatures  $T_c^{dR/dT}$  estimated by the position of maximum of dR(T)/dT (lines in the lower insets of Figure 1) are equal to approx.  $30.3\,\mathrm{K}$  (width of the SC-transition is  $\Delta T_c\approx 0.7\,\mathrm{K}$ ) for KNFS and  $25.5\,\mathrm{K}$  ( $\Delta T_c\approx 1.1\,\mathrm{K}$ ) for KFSS, and according to the magnetic susceptibility measurements (upper insets of Figure 1, a and b) —  $T_{c,\chi}^{\mathrm{onset}}\approx 29.3$  and  $24.5\,\mathrm{K}$ , respectively.

Structure of the SC order parameter was determined using the IMARE spectroscopy. This effect occurs below  $T_c$  in a so-called "long" superconductor — thin normal metal — superconductor (SnS) contact without phase coherence between the SC-banks (where the contact diameter d exceeds the coherence length  $\xi_0$  [23–25]. In a high transparency mode of nS-boundaries (barrier parameter Z < 0.3), the current-voltage curve (CVC) of the SnScontact has no supercurrent branch at eV = 0, and excess current occurs across the entire bias voltage range eVcompared with CVC in the normal state [23,24]. At low bias voltages, a higher, however, finite slope (a so-called "foot") region is observed in the CVC with the number of the Andreev reflections limited by a typical inelastic scattering time. Beginning of the "foot" is accompanied by a sudden variation of the CVC slope with  $eV \rightarrow 0$  and may induce a minimum with  $V = V_{\text{foot}}$  in the corresponding dI(V)/dVspectrum [15]. Unlike the subharmonic gap structure (SGS) minima  $V_n$ , the position of  $V_{\text{foot}}$  doesn't define directly the SC-gap amplitude:  $V_{\text{foot}}$  depends on l/d of a particular contact (l is the typical inelastic scattering length) and is close to  $V_{\text{foot}} \approx V_1 \cdot d/l$  by order of magnitude according to the formalism of [24,25].

The magnitude of the microscopic SC order parameter  $\Delta(T)$  defines directly the subharmonic gap structure (SGS) positions — series of the  $\mathrm{d}I(V)/\mathrm{d}V$  minima with positions  $|\mathrm{e}V_n(T)| = 2\Delta(T)/n$ , where  $n=1, 2, \ldots$  — at any temperatures up to  $T_c$  [23,24]. The number  $n^*$  of the observed SGS minima for a planar contact (in case of Z=0 and zero broadening parameter) corresponds approximately to  $n^* \approx l_c/d_c$  (both quantities are taken along

the c-direction) [23–26] and decreases as Z and inelastic scattering increase.

A planar mechanically-adjustable modification [27] of the "break-junction" technique [28] developed for layered compound samples was used to make SnS contacts in ferroselenide crystals. Experiment configuration and the types of obtained tunneling structures, advantages and disadvantages of the method are described in detail in the review [27]. A rectangular sample with dimensions about  $3 \times 1.5 \times 0.2 \,\mathrm{mm}^3$  is mounted on a  $\Pi$ -shaped holder according to a 4-point scheme with the crystallographic ab-plane oriented parallel to the holder and cooled to  $T = 4.2 \,\mathrm{K}$ . During precision bending of the holder, a microcrack is formed in the sample to serve as a tunneling barrier between two bulk SC-banks. The obtained tunneling mode is real-time controlled on the basis of the CVC shape. Since the mean width of SC crystallites in ferroselenides  $(\sim 1 \,\mu\text{m})$  is much larger than the estimated size of the tunneling junction ( $d \approx 10-50 \,\mathrm{nm}$ ), then the microcrack may pass within the SC region; in this case for the studied selenides, formation of SnS contacts in the hightransparency IMARE mode is more typical.

It is known that steps and terraces form at the cleaved surfaces of any layered compounds. During the experiment, the contact banks are not separated at a considerable distance to prevent impurity penetration and degradation of cryogenic clefts. The crack remains within the sample, and the tunneling junction is formed between the touching terraces. Thus, measurement current through the prepared planar contact always passes along the crystallographic c-direction. During fine mechanical adjustment of the holder bend, junctions with different area in the ab-plane and normal resistance  $R_{\rm N}$  (at  $eV\gg 2\Delta(0)$ ) may be formed. The observed bulk energy characteristics of the SC subsystem shall not obviously depend on  $R_{\rm N}$ , which is a random variable for contacts on microcrack.

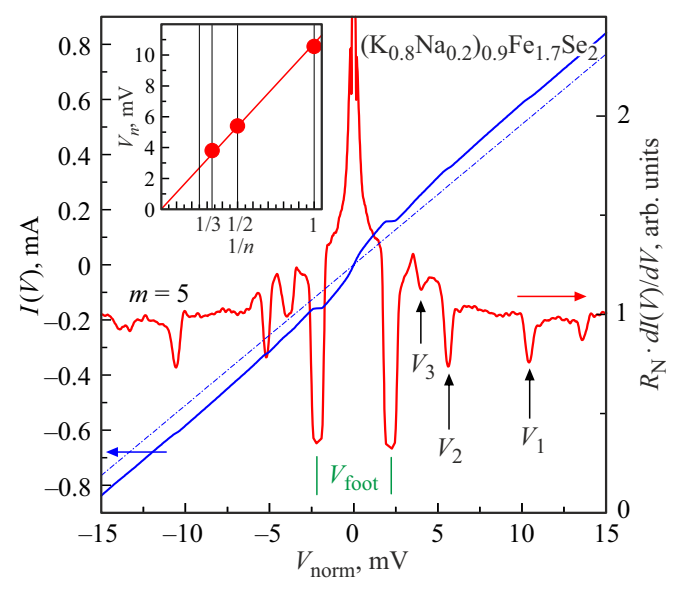
Besides single SnS contacts, formation of SnSn-...-S stack structures consisting of SnS contacts with almost the same  $R_N$  on the steps and terraces of the cryogenic cleaved faces of layered materials is typical for the employed technique. When such stack consisting of m contacts (where m is an integer) is obtained, positions of any features defined by bulk energy parameters of superconductor will be m times as high as those for a single SnS contact:  $|eV_n(T)| = 2m\Delta(T)/n$ . The number m of contacts in the stack can be unambiguously determined by collecting statistical data and comparing the dI(V)/dV-spectra of the stacks with a different, though small (usually m < 20) number of contacts (for example, according to a procedure described in the appendix to [29]). For CVC and dI(V)/dVspectra provided in the work, the bias voltage axis is divided into the corresponding m:  $V_{\text{norm}} = V/m$ . As reported previously [27,29], the share of bulk effects in a stack structure increases, and the contribution of surface effects decreases with the growth of m, which provides better dI(V)/dV-spectra.

Summing up, note that the IMARE spectroscopy method implemented in the mechanically adjustable planar SnS break-junctions and stack SnSn-...-S structures provides direct local measurement of the SC order parameter and its temperature dependence. Fine tuning of the microcrack may be used to get dozens of SnS and SnSn-...-S structures with various  $R_{\rm N}$  per contact, which facilitates collecting statistical data and verifying data repeatability.

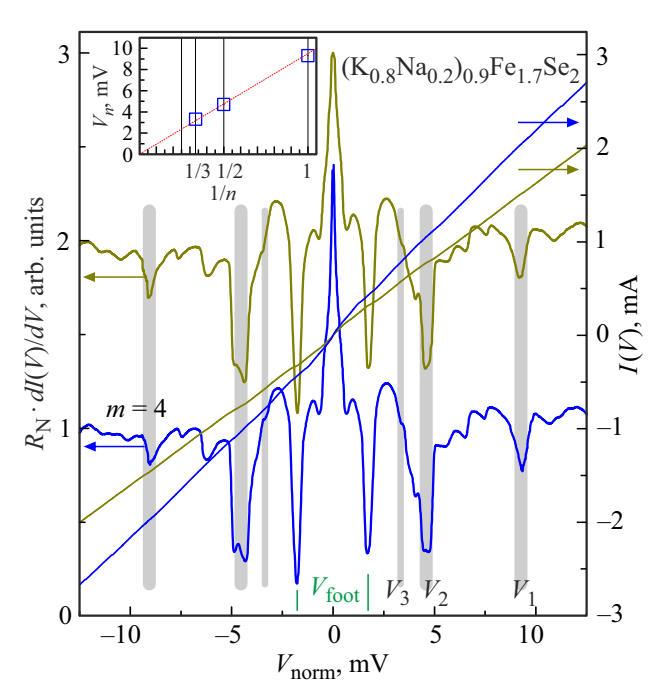
## 3. Experimental results

Figure 2 shows CVC and dI(V)/dV-spectrum of the stack SnS contact (m = 5) in the KNFS crystal measured at  $T = 4.2 \,\mathrm{K}$ . The given CVC was measured in two directions using a DC current source, is almost symmetric with respect to eV = 0, doesn't contain a supercurrent branch and hystereses. CVC clearly shows an excess current with respect to the ohmic dependence throughout the bias voltage eV range and an increased slope region with small biases ("foot"), which indicates that the hightransparency IMARE mode is realized in accordance with all existing theoretical representations [23–26]. The dynamic conductance spectrum clearly shows minima at bias voltages  $|V_1| \approx 10.5 \,\text{mV}, |V_2| \approx 5.5 \,\text{mV}$  and  $|V_3| \approx 3.8 \,\text{mV}$ . These features may be interpreted as n = 1, 2, 3 order subharmonics because their position almost linearly depends on the corresponding inverse number 1/n as shown in the inset in Figure 2. On average, the observed SGS defines the SC gap magnitude  $2\Delta(0) \approx 11$  meV. Intense minima at small bias voltages  $|V| \approx 2.2 \,\mathrm{mV} = V_{\mathrm{foot}}$  correspond to a drastic change of CVC slope (beginning of the "foot") and are not a subharmonic of any order of the same SC gap and also cannot be interpreted as the beginning of the second SGS (n = 1) from a hypothetically small SC gap for the reasons discussed below. At larger bias voltages,  $|V| = 13-14 \,\mathrm{mV}$ , the spectrum has an out-ofgap fine structure that was presumably induced by the resonance interaction of electrons in the IMARE process with a typical boson mode. This structure is similar to that observed earlier in iron-containing superconductors from other families [29,30] and needs additional thorough investigation.

CVC and dI(V)/dV-spectra of SnS structures (m=4) measured in the same KNFS crystal at  $T=4.2\,\mathrm{K}$  successively by means of fine tuning are shown in Figure 3. It is shown that  $R_{\mathrm{N}}$  and, consequently, the area of these contacts as well differ by  $\sim 35\,\%$ , which can be seen by the CVC slope change at large bias voltages; however, the shape of the dI(V)/dV-spectrum and position of all features remained unchanged. Minima at  $|V|\approx 9.3$  and  $4.7\,\mathrm{mV}$ , and less pronounced features at  $|V|\approx 9.3\,\mathrm{mV}$  form SGS of the SC gap with magnitude  $2\Delta(0)\approx 9.5\,\mathrm{meV}$ . Linear dependence of positions of these features on their inverse number passing also through the origin of coordinates is shown in the inset in Figure 3.



**Figure 2.** Current-voltage curve (left vertical axis, blue line) and dI(V)/dV-spectrum (right axis, red line) of a SnS Andreev contact stack (m=5), measured at  $T=4.2\,\mathrm{K}$  in the  $(\mathrm{K_{0.8}Na_{0.2}})_{0.9}\mathrm{Fe_{1.7}Se_2}$  crystal. Dotted and dashed line is the corresponding ohmic dependence. Arrows show positions  $V_n$  of n=1, 2, 3 order Andreev subharmonics of the SC-gap  $2\Delta(0)\approx 11\,\mathrm{meV}$ , green vertical bars show the "foot" position  $V_{\mathrm{foot}}$ . The inset shows the dependence of the SGS features positions  $V_n$  on their inverse number 1/n.



**Figure 3.** Current-voltage curve (left vertical axis) and dI(V)/dV-spectra (right axis) of the SnS Andreev stack contacts (m=4) measured at  $T=4.2\,\mathrm{K}$  in the same  $(\mathrm{K}_{0.8}\mathrm{Na}_{0.2})_{0.9}\mathrm{Fe}_{1.7}\mathrm{Se}_2$  crystal. Local critical contact temperature is  $T_c^{\mathrm{local}}\approx 25\,\mathrm{K}$ . Grey vertical lines show the positions  $V_n$  of n=1,2,3 order Andreev subharmonics from the SC-gap  $2\Delta(0)\approx 9.5\,\mathrm{meV}$ , green bars show the beginning of the "foot"  $V_{\mathrm{foot}}$ . The inset shows the dependence of the positions of the SGS  $V_n$  on their inverse number 1/n.

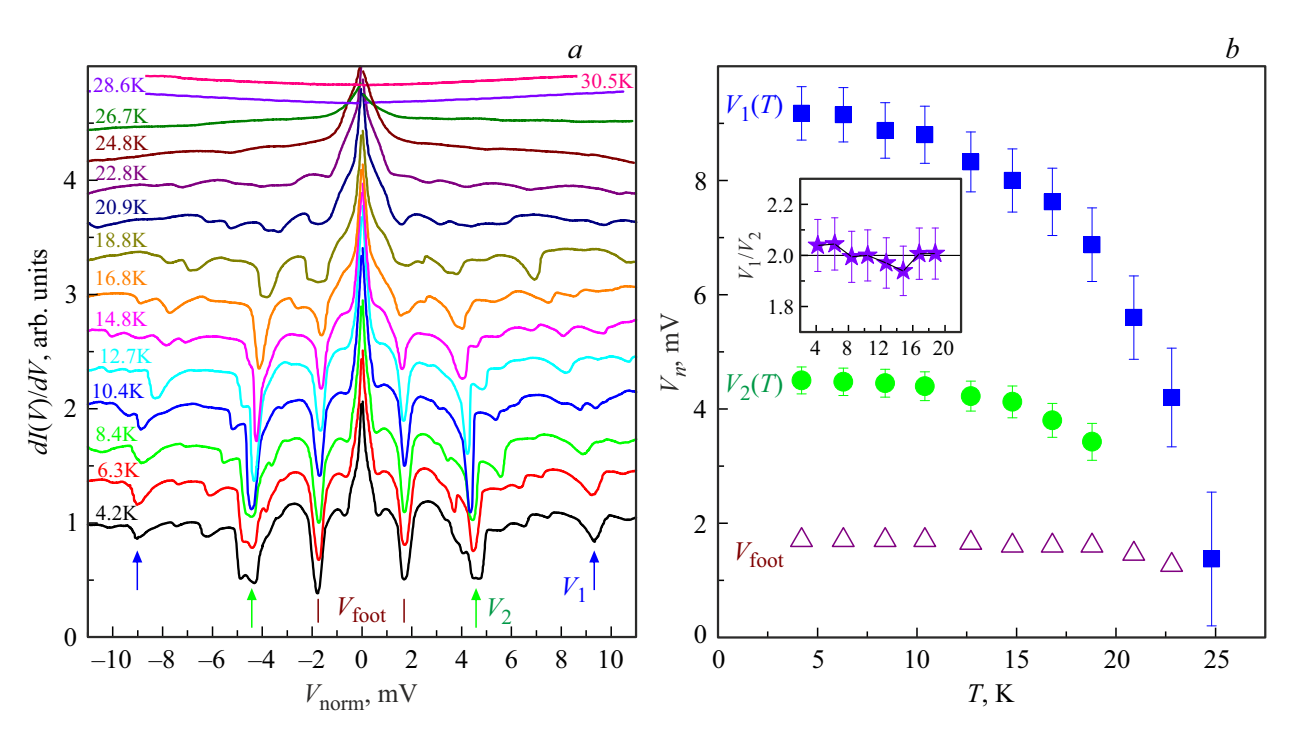


**Figure 4.** *a*) Dynamic conductance spectrum of the SnS Andreev contact formed in the  $(K_{0.8}Na_{0.2})_{0.9}Fe_{1.7}Se_2$  sample (shown in Figure 3 in blue) measured at  $4.2 \le T \le 30.5$  K in SC and normal state. Spectra were vertically shifted manually for clarity. Arrows at T = 4.2 K mark the position of the n = 1, 2 Andreev minima of the SC order parameter  $2\Delta(0) \approx 9.5$  meV. *b*) Dependence of the Andreev harmonic positions  $V_1$  (squares),  $V_2$  (circles) on temperature according to (a). For comparison, triangles show the temperature behavior of the feature at  $V_{\text{foot}}(0) \approx 1.8$  mV that doesn't pertain to SGS and is interpreted as the beginning of the "foot".

Temperature evolution of the dI(V)/dV-spectrum shown in Figure 3 is given in Figure 4, a. For convenience, the spectra in Figure 4, a were vertically shifted manually with increase in temperature, whereby for this contact  $R_{\rm N}(T) \approx {\rm const.}$  As the temperature increases, the position of SGS minima shifts towards zero, zero-bias conductance also decreases ("foot" amplitude). At  $T = 28.6 \,\mathrm{K}$ , the spectrum is linearized, which means that the contact region switches to a normal state and the IMARE-induced features disappear. Positions of the fundamental harmonic  $V_1(T)$ and second subharmonic  $V_2(T)$  of the SC gap in the dependence on temperature are shown as squares and circles, respectively, in Figure 4, b. These dependences are similar to each other: as shown in the inset in Figure 4, b, relation of the SGS minima positions n = 1 and n = 2 is approximately equal to two in a wide temperature range in accordance with the equation for SGS [23,24,26]. On the contrary, minima at  $V_{\text{foot}}$  demonstrate a weak temperature dependence that doesn't correspond to that for the Andreev subharmonics (triangles in Figure 4, b), therefore their position doesn't directly define  $\Delta(T)$ .

CVC and dynamic conductance spectra of the planar stack contacts on microcrack obtained by successive adjustment in the same KFSS crystal at  $T=4.2\,\mathrm{K}$  are shown in Figure 5. The spectra have SGS consisting of our features at mean bias voltages  $|V_1|\approx 10.1\,\mathrm{mV}$ ,  $|V_2|\approx 4.7\,\mathrm{mV}$ ,  $|V_3|\approx 3.3\,\mathrm{mV}$ ,  $|V_4|\approx 2.3\,\mathrm{mV}$ . According to the slope of  $V_n(1/n)$  shown in the inset in Figure 5, b, the

SC gap magnitude  $2\Delta(0) \approx 9.7 \,\mathrm{meV}$  may be determined. It can be seen that after normalization to the integers  $m=10,\ 11,\ 13$ , the shape of spectrum and feature positions are reproduced with high accuracy: spread of  $V_n$  (n=1-4) of the SGS features doesn't exceed  $\pm 6\,\%$ , while the normal resistance variation per contact is about  $20\,\%$  (see the CVC slope in Figure 5, b). Consequently, it may be concluded that the observed SGS features cannot be explained by dimensional resonances or random effects.

Temperature evolution of the dI(V)/dV-spectrum of the SnS-contact (m=5) formed in the KFSS crystal is shown in Figure 6. Similar to Figure 4, curves in Figure 6 are deliberately shifted vertically for clarity, while the normal resistance of this contact remains almost unchanged with temperature. The most strong minima (marked at  $T=4.2\,\mathrm{K}$  as  $2\Delta$ ) are the fundamental Andreev harmonic of the SC order parameter  $2\Delta(0)\approx 8.4\,\mathrm{meV}$ . At  $T=26.5\,\mathrm{K}$ , all IMARE-induced features on the spectrum vanish indicating that the superconductivity disappears locally at  $T>T_c^{\mathrm{local}}$  and the Copper pairs are destroyed.

Figure 7, a and b shows the SC-gap temperature dependences plotted using the data in Figure 4 (triangles with cusps upwards, a) and Figure 6 (triangles with cusps downwards, b), and the similar data on the basis of the measurements of  $\mathrm{d}I(V)/\mathrm{d}V$ -spectra of other SnS contacts made in the KNFS (a) and KFSS (b) crystals. Within errors, all experimental dependences  $\Delta(T)$  (symbols in Figure 7, a

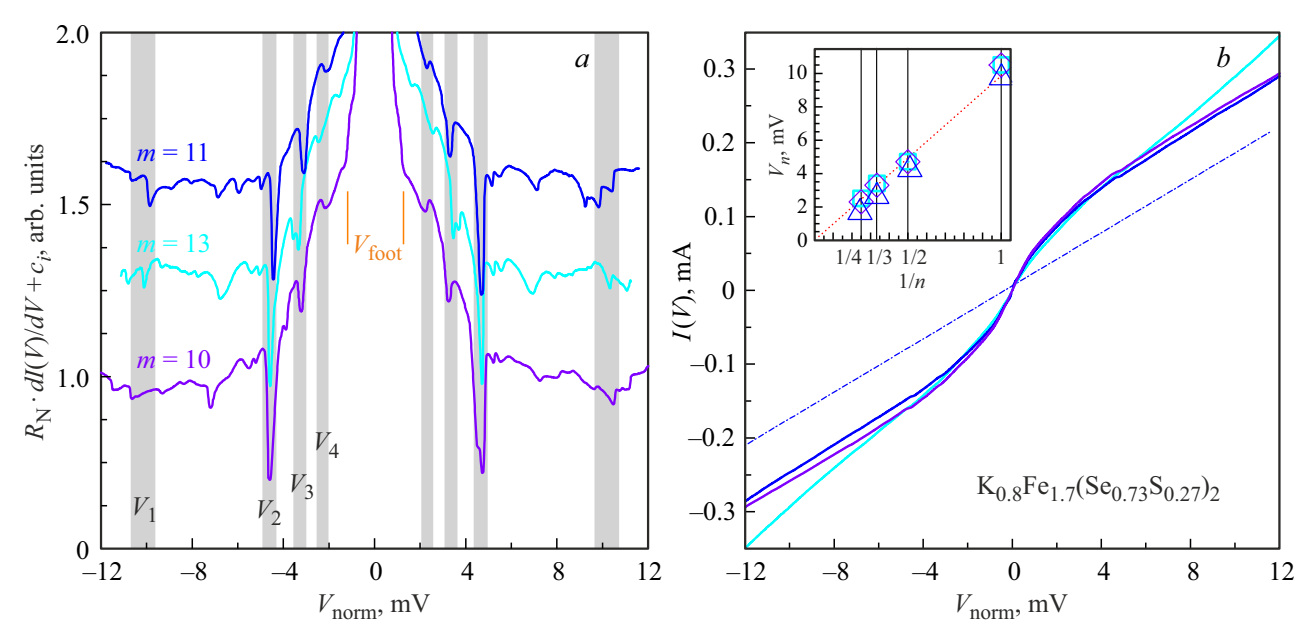
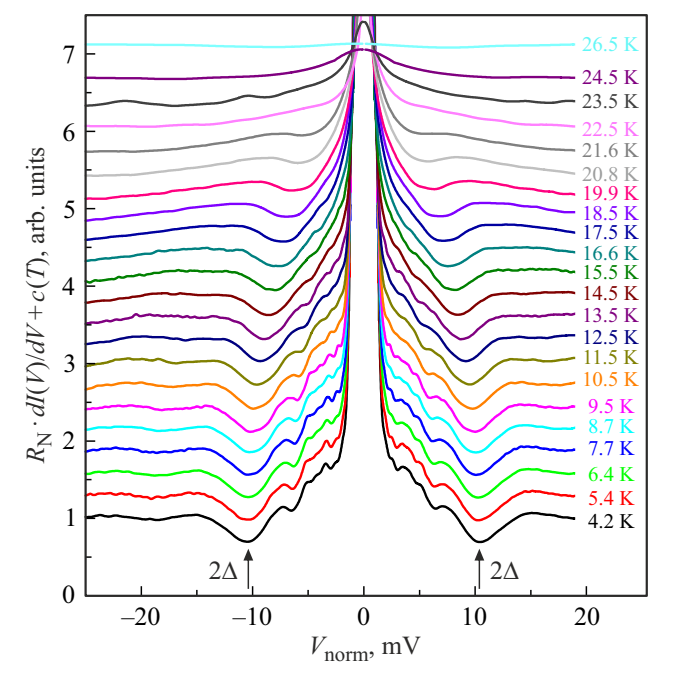


Figure 5. a) dI(V)/dV spectra of stack SnS Andreev contacts (m = 10, 11, 13) obtained at T = 4.2 K in the same  $K_{0.8}Fe_{1.7}(Se_{0.73}S_{0.27})_2$  sample. Grey vertical lines show the positions  $V_n$  of the n = 1, 2, 3, 4 order Andreev subharmonics of the SC-gap  $2\Delta(0) \approx 9.7$  meV, orange bars show the beginning of the "foot"  $V_{\text{foot}}$ . b) CVC of these contacts. Dotted and dashed line is the ohmic dependence corresponding to the blue CVC. The inset shows the dependence of the positions of the SGS features  $V_n$  on their inverse number 1/n.

and b) agree well with single-band functions similar to the SC-gap temperature dependence within the framework of the Bardeen-Cooper-Schrieffer (BCS) model (dotted and dashed lines with corresponding colors). Local critical



**Figure 6.** dI(V)/dV-spectrum of the SnS Andreev contact in the  $K_{0.8}Fe_{1.7}(Se_{0.73}S_{0.27})_2$  sample measured at  $4.2 \le T \le 26.5$  K. Spectra were vertically shifted manually for clarity. Arrows at T=4.2 K show the fundamental Andreev harmonic position from the SC order parameter  $2\Delta(0)\approx 8.4$  meV.

temperatures of the junctions  $T_c^{\rm local}$  (meaning transition of this  $\sim 10-50\,{\rm nm}$  region to the normal state) are estimated as temperatures at which the BCS-like approximation curves vanish. To compare  $\Delta(T)$  obtained for various samples and SnS structures with variation of absolute values  $\Delta(0)$  and  $T_c^{\rm local}$  in Figure 7, c, the obtained data is shown in the normalized coordinates  $2\Delta(T)/k_{\rm B}T_c$  on  $T/T_c^{\rm local}$ . It can be seen that the single-band BCS-like dependence trend is well reproduced for KNFS and KFSS, and when  $T\ll T_c$ , all obtained data is within  $2\Delta(0)/k_{\rm B}T_c\approx 4.1-4.6$ .

## 4. Discussion

IMARE experiments provided a significant amount of statistical data on the magnitude of  $2\Delta(0)/k_BT_c$  of the SC-gap observed in KNFS (blue) and KFSS (red) shown in Figure 8, a-f. Figure 8, a shows the histograms of  $2\Delta(0)/k_{\rm B}T_c$  obtained from the studies of I(V) and dI(V)/dV-characteristics of the SnS structures in KNFS (a) and KFSS (b). Data for each contact is shown as a semitransparent column whose horizontal position corresponds to  $2\Delta(0)/k_{\rm B}T_c$ . Most commonly observed experimental values (regions with the maximum color intensity in Figure 8, a and b)  $-2\Delta(0)/k_BT_c \approx 4.2$  for KNFS and  $2\Delta(0)/k_BT_c = 4.2-4.4$  for KFSS. Full ranges of the measured characteristic ratios for KNFS and KFSS are close to each other and equal to  $2\Delta(0)/k_BT_c = 4.1-4.6$ . For each compound, the spread of values doesn't exceed ±6%, which confirms high accuracy of the used IMARE spectroscopy method. The characteristic ratios exceeding the BCS weak coupling limit 3.53 indicate that strong

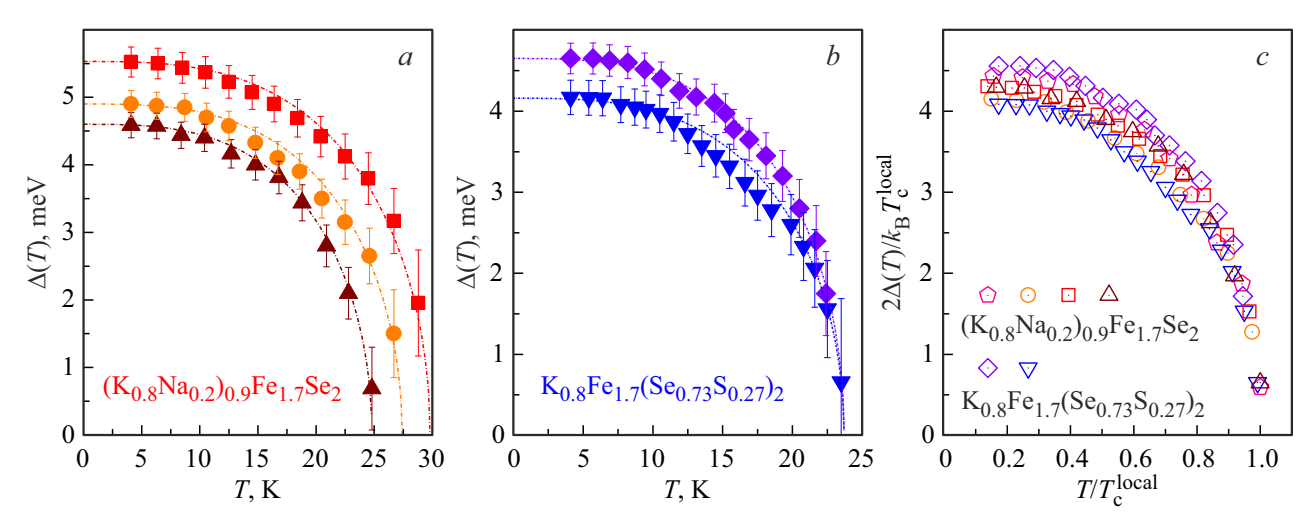


**Figure 7.** Temperature dependences of the SC gap  $\Delta(T)$  according to the measurements of dI(V)/dV-spectra of various SnS contacts on the basis of a) (K<sub>0.8</sub>Na<sub>0.2</sub>)<sub>0.8</sub>Fe<sub>1.7</sub>Se<sub>2</sub> and b) K<sub>0.8</sub>Fe<sub>1.7</sub>(Se<sub>0.73</sub>S<sub>0.27</sub>)<sub>2</sub>. Dotted and dashed lines show approximations by single-band BCS-like functions,  $T_c^{local}$  of each contact was determined as a temperature at which the corresponding approximation  $\Delta(T)$  vanishes. c) Normalized dependences  $2\Delta(T)/k_BT_c$  on  $T/T_c^{local}$  for the shown contacts.

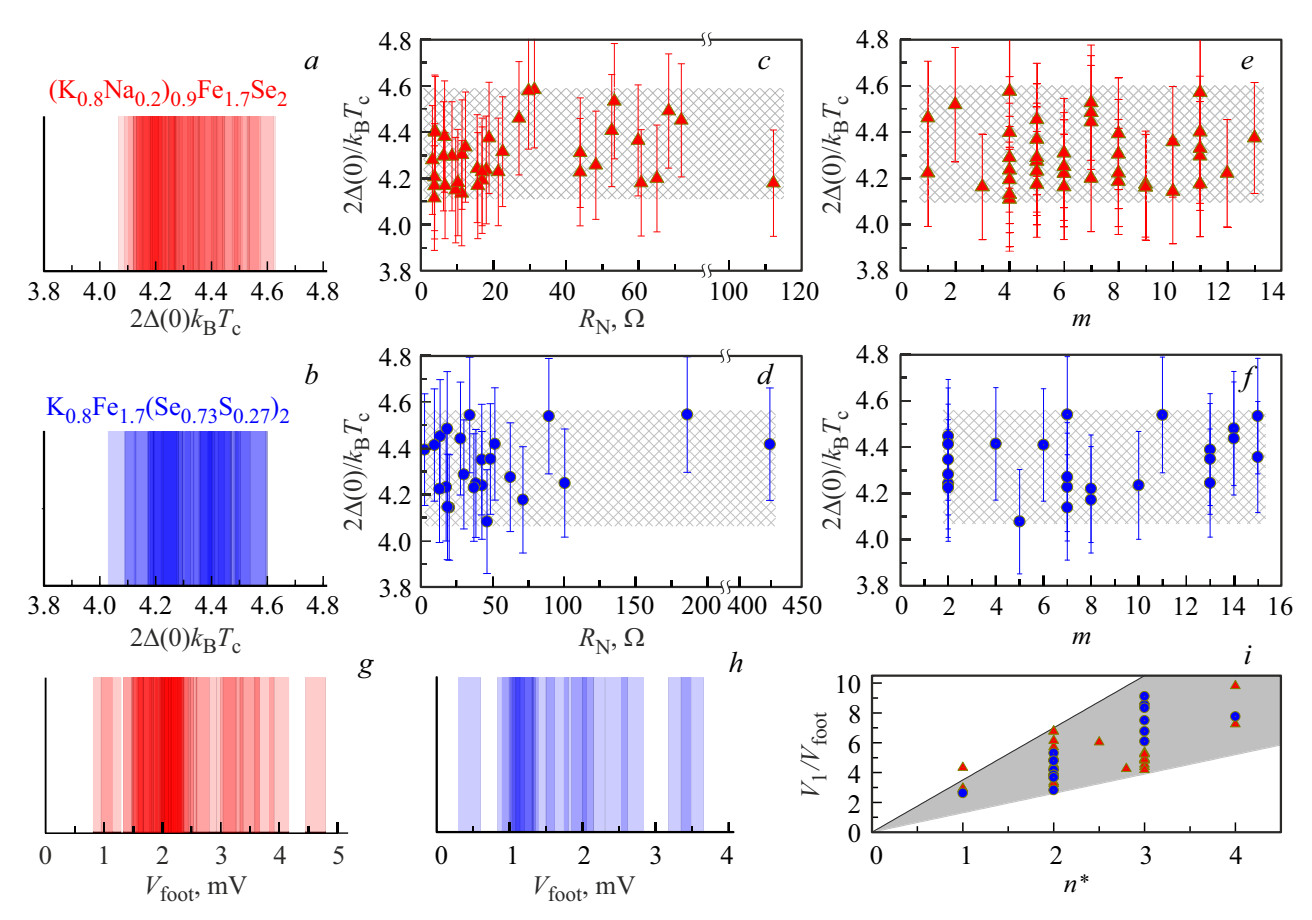


**Figure 8.** a and b) Histograms of the characteristic ratios of the SC-gap  $2\Delta(0)/k_BT_c$  for  $(K,Na)_xFe_{2-y}Se_2$  and  $K_zFe_{2-y}(Se,S)_2$ , respectively. Each value is represented as a semitransparent column whose position corresponds to  $2\Delta(0)/k_BT_c$ ; the most intense color region shows a value that is most frequently obtained in the experiment. Vertical axis has no value. (c-f) Dependences of  $2\Delta(0)/k_BT_c$  on normal contact resistance  $R_N$  (c and d) and on the number of contacts in the stack m of the corresponding SnS structure (e and f) for KNFS (e and e) and KFSS (e and e) Statistics of "foot" positions: histograms of  $V_{foot}$  bias voltages in KNFS (e) and KFSS (e), relation of the fundamental harmonic position  $V_1$  to  $V_{foot}$  on the number e0 subharmonics (e1) observed on the e1 of e2.

coupling occurs in the Copper pairs formed below  $T_c$  in the KNFS and KFSS electron bands.

The obtained values  $2\Delta(0)/k_BT_c=4.1-4.6$  are reproduced on various samples from the same batch and don't correlate either with the normal resistance  $R_{\rm N}$  per contact (Figure 8, c and d) or with the number of contacts in the stack m (Figure 8, e and f). Thus, the obtained energy parameters of a superconductor don't depend on the properties of the studied contact; on the contrary, they describe the fundamental SC-properties of a material. Repeatability of  $\Delta(0)$  and  $2\Delta(0)/k_BT_c$  in the investigation of stack SnSn-...S structures with different m proves the bulk nature of the observed SC order parameter.

Let's review the statistics of positions of minima often observed on the dI(V)/dV-spectra at small bias voltages  $V_{\text{foot}} \ll V_1$  (see Figure 2–5). Taking into account their significant amplitude (exceeding considerably that for high order subharmonics  $V_3$ ,  $V_4$  of the SC-gap), may these features be classified, for example, as the fundamental Andreev harmonic from any SC-gap? We put forward some arguments against this assumption. First, the positions  $V_{\rm foot}$  demonstrate a considerable spread that is by orders of magnitude larger than that for gap features (Figure 8, g-i):  $V_{\text{foot}} = 0.9 - 4.6 \,\text{mV}$  in KNFS (i.e. their position varies more than fivefold, see Figure 8, g) and  $V_{\text{foot}} = 0.5 - 3.5 \,\text{mV}$ in KFSS (approximately sevenfold, see Figure 8, h). Second,  $V_1/V_{\rm foot}$  correlates with  $n^*$  of subharmonics observed on the spectrum: except the "escaped" points, all obtained data forms a sector. This agrees qualitatively with classical predictions [24,25] for the "foot" position — a dynamic conductance minimum that occurs when the CVC slope is changed suddenly at small bias voltages and marks the beginning of a region where the Andreev process dynamics is controlled by inelastic scattering to a greater extent. Finally, a weaker temperature dependence  $V_{\text{foot}}(T)$  (see Figure 4, b) that doesn't follow the trend  $\Delta(T)$  shall be considered. The above-mentioned arguments may be used to make a conclusion that positions of these minima don't define directly the SC-gap magnitude and are associated with  $l_c/d_c$  of the contact, rather than of the properties of the studied superconductor.

Thus, in particular, the minima at small bias voltages  $V_{\rm foot} \ll V_1$  cannot be a fundamental (n=1) harmonic from a hypothetical small SC gap  $\Delta_S \ll \Delta$ . Along with the repeatedly observed BCS-like temperature dependence  $\Delta(T)$  (see Figure 7), this allows a conclusion to be made that the only one SC order parameter exists in KNFS and KFSS. In other words, regardless of the presence/absence of an electron pocket in  $\Gamma$ -point (detection of which is the objective of future ARPES investigations), common SC condensate develops on all sheets of Fermi surface below  $T_C$ .

Most iron-containing superconductors are known to demonstrate multicomponent superconductivity below  $T_c$  (simultaneous existence of several types of Copper pairs in any point of the real space). From this point of view, a development of the conventional single-gap superconductivity in the studied ferroselenides with isovalent substitution

seems to be unusual itself. Comparing some aspects of the properties of studied  $A_x$ Fe<sub>2</sub>Se<sub>2</sub> (KNFS and KFSS) and related pnictides of the AeFe<sub>2</sub>As<sub>2</sub> family (Ae is an alkaline earth metal), the following paradox may be also noted. Though, AeFe<sub>2</sub>As<sub>2</sub> pnictides feature a relative simplicity of structural properties, structure of their SC order parameter is extremely sophisticated because its magnitude likely depends on the momentum direction (anisotropy in the k-space) [31,32]. On the contrary, in case of  $A_r \text{Fe}_2 \text{Se}_2$ , the simplest SC-gap structure develops in so complex multiphase compounds with non-trivial [3] coupling  $T_c$  with composition variation that is defined to a greater extent by chemical pressure, rather than by the concentration of doping electrons [3,4,7,8]. When addressing the observed unification of the SC order parameter in various KNFS and KFSS bands, then within a multiple-band approximation of the BCS theory [33,34], an assumption may be made concerning a single mechanism of both intraband and interband pairing, unlike the AeFe<sub>2</sub>As<sub>2</sub> SC system.

## 5. Conclusion

Incoherent multiple Andreev reflection effect spectroscopy methods below  $T_c$  were used to determine the structure of the SC order parameter of  $(K_{0.8}Na_{0.2})_{0.9}Fe_{1.7}Se_2$  and  $K_{0.8}Fe_{1.7}(Se_{0.73}S_{0.27})_2$ . A similar SC-gap structure with the only one SC-gap that develops below  $T_c$  was established in both materials. Bulk nature of the observed SC order parameter is shown. Temperature dependence  $\Delta(T)$  agrees with the BCS-like function.  $2\Delta(0)/k_BT_c=4.35\pm0.25$  is reproduced for both materials and indicates that strong coupling is realized in electron bands.

#### **Acknowledgments**

The study was supported by the project of the Russian Science Foundation No. 22-72-10082. The measurements were partially done using the equipment provided by the Shared Research Facility of Lebedev Physical Institute, Russian Academy of Sciences.

#### Conflict of interest

The authors declare no conflict of interest.

## References

- J. Guo, S. Jin, G. Wang, S. Wang, K. Zhu, T. Zhou, M. He, X. Chen. Phys. Rev. B 82, 18, 180520(R) (2010).
- [2] E. Dagotto. Rev. Mod. Phys. 85, 2, 849 (2013).
- [3] A. Krzton-Maziopa, V. Svitlyk, E. Pomjakushina, R. Puzniak, K. Conder. J. Phys.: Condens. Matter **28**, *29*, 293002 (2016).
- [4] A. Krzton-Maziopa. Front. Chem. 9, 640361 (2021).
- [5] D. Croitori, I. Filippova, V. Kravtsov, A. Günther, S. Widmann, D. Reuter, H.-A. Krug von Nidda, J. Deisenhofer, A. Loidl, V. Tsurkan. Phys. Rev. B 101, 5, 054516 (2020).

- [6] X.-W. Yan, M. Gao, Z.-Y. Lu, T. Xiang. Phys. Rev. B 84, 5, 054502 (2011).
- [7] H. Lei, M. Abeykoon, E.S. Bozin, K. Wang, J.B. Warren,C. Petrovic. Phys. Rev. Lett. 107, 13, 137002 (2011).
- [8] P. Mangelis, R.J. Koch, H. Lei, R.B. Neder, M.T. Mc-Donnell, M. Feygenson, C. Petrovic, A. Lappas, E.S. Bozin. Phys. Rev. B 100, 9, 094108 (2019).
- [9] M.M. Korshunov. Phys. Uspekhi 57, 8, 813 (2014).
- [10] M. Xu, Q.Q. Ge, R. Peng, Z.R. Ye, J. Jiang, F. Chen, X.P. Shen, B.P. Xie, Y. Zhang, A.F. Wang, X.F. Wang, X.H. Chen, D.L. Feng. Phys. Rev. B 85, 22, 220504(R) (2012).
- [11] D. Mou, S. Liu, X. Jia, J. He, Y. Peng, L. Zhao, L. Yu, G. Liu, S. He, X. Dong, J. Zhang, H. Wang, C. Dong, M. Fang, X. Wang, Q. Peng, Z. Wang, S. Zhang, F. Yang, Z. Xu, C. Chen, X.J. Zhou. Phys. Rev. Lett. 106, 10, 107001 (2011).
- [12] J. Maletz, V.B. Zabolotnyy, D.V. Evtushinsky, A.N. Yaresko, A.A. Kordyuk, Z. Shermadini, H. Luetkens, K. Sedlak, R. Khasanov, A. Amato, A. Krzton-Maziopa, K. Conder, E. Pomjakushina, H.-H. Klauss, E.D.L. Rienks, B. Büchner, S.V. Borisenko. Phys. Rev. B 88, 13, 134501 (2013).
- [13] Y. Zhang, L.X. Yang, M. Xu, Z.R. Ye, F. Chen, C. He, H.C. Xu, J. Jiang, B.P. Xie, J.J. Ying, X.F. Wang, X.H. Chen, J.P. Hu, M. Matsunami, S. Kimura, D.L. Feng. Nature Mater. 10, 4, 273 (2011).
- [14] X.-P. Wang, T. Qian, P. Richard, P. Zhang, J. Dong, H.-D. Wang, C.-H. Dong, M.-H. Fang, H. Ding. EPL 93, 5, 57001 (2011).
- [15] L.L. Lev, T.E. Kuzmicheva, S.A. Kuzmichev, A.M. Lebedev, V.G. Nazin, R.G. Chumakov, A.I. Shilov, E.O. Rahmanov, I.V. Morozov. Moscow Univ. Phys. Bull. 79, 2410502 (2024).
- [16] I.I. Mazin, D.J. Singh, M.D. Johannes, M.H. Du. Phys. Rev. Lett. 101, 5, 057003 (2008).
- [17] H. Kontani, S. Onari. Phys. Rev. Lett. 104, 15, 157001 (2010).
- [18] S. Maiti, M.M. Korshunov, T.A. Maier, P.J. Hirschfeld, A.V. Chubukov. Phys. Rev. B 84, 22, 224505 (2011).
- [19] M. Khodas, A.V. Chubukov. Phys. Rev. Lett. 108, 24, 247003 (2012).
- [20] T. Saito, S. Onari, H. Kontani. Phys. Rev. B 83, 14, 140512(R) (2011).
- [21] L. Benfatto, B. Valenzuela, L. Fanfarillo. npj Quantum Mater. 3, 1, 56 (2018).
- [22] E.M. Nica, R. Yu, Q. Si. npj Quantum Mater. 2, 1, 24 (2017).
- [23] M. Octavio, M. Tinkham, G.E. Blonder, T.M. Klapwijk. Phys. Rev. B 27, 11, 6739 (1983).
- [24] R. Kümmel, U. Gunsenheimer, R. Nicolsky. Phys. Rev. B 42, 7, 3992 (1990).
- [25] U. Gunsenheimer, A.D. Zaikin. Europhys. Lett. 41, 2, 195 (1998).
- [26] Z. Popović, S. Kuzmichev, T. Kuzmicheva. J. Appl. Phys. 128, 1, 013901 (2020).
- [27] S.A. Kuzmichev, T.E. Kuzmicheva. Low Temp. Phys. 42, 11, 1008 (2016).
- [28] J. Moreland, J.W. Ekin. J. Appl. Phys. 58, 10, 3888 (1985).
- [29] T.E. Kuzmicheva, S.A. Kuzmichev, N.D. Zhigadlo. Phys. Rev. B 100, 14, 144504 (2019).
- [30] M.M. Korshunov, S.A. Kuzmichev, T.E. Kuzmicheva. Mater. 15, 17, 6120 (2022).
- [31] D.V. Evtushinsky, V.B. Zabolotnyy, L. Harnagea, A.N. Yaresko, S. Thirupathaiah, A.A. Kordyuk, J. Maletz, S. Aswartham, S. Wurmehl, E. Rienks, R. Follath, B. Büchner, S.V. Borisenko. Phys. Rev. B 87, 9, 094501 (2013).

- [32] T.E. Kuzmicheva, Yu.A. Aleshchenko, P.I. Bezotosnyi, S.Yu. Gavrilkin, K.A. Dmitrieva, A.D. Ilina, S.A. Kuzmichev, A.V. Muratov, I.A. Nikitchenkov, G.V. Rybalchenko. JETP Lett. 121, 6, 441 (2025).
- [33] V.A. Moskalenko. Phys. Met. Metallogr. 8, 25 (1959).
- [34] H. Suhl, B.T. Matthias, L.R. Walker. Phys. Rev. Lett. 3, 12, 552 (1959).

Translated by E.Ilinskaya